A Measurement of the Cosmic Ray Spectrum and Composition at the Knee

J.W. Fowler [a,1] L.F. Fortson [a,b] C.C.H. Jui [c] D.B. Kieda [c]
R.A. Ong [a] C.L. Pryke [a] P. Sommers [c]

[a] *The Enrico Fermi Institute, University of Chicago, 5640 Ellis Avenue, Chicago, Illinois 60637-1433, USA*

[b] *Dept. of Astronomy, Adler Planetarium and Astronomy Museum, Chicago, Illinois 60605, USA*

[c] *High Energy Astrophysics Institute, Dept. of Physics, University of Utah, Salt Lake City, Utah 84112, USA*

The energy spectrum and primary composition of cosmic rays with energy between 3×10^{14} and 3×10^{16} eV have been studied using the CASA-BLANCA detector. CASA consisted of 957 surface scintillation stations; BLANCA consisted of 144 angle-integrating Cherenkov light detectors located at the same site. CASA measured the charged particle distribution of air showers, while BLANCA measured the lateral distribution of Cherenkov light. The data are interpreted using the predictions of the CORSIKA air shower simulation coupled with four different hadronic interaction codes.

The differential flux of cosmic rays measured by BLANCA exhibits a knee in the range of 2–3 PeV with a width of approximately 0.5 decades in primary energy. The power law indices of the differential flux below and above the knee are -2.72 ± 0.02 and -2.95 ± 0.02, respectively.

We present our data both as a mean depth of shower maximum and as a mean nuclear mass. A multi-component fit using four elemental species suggests the same composition trends exhibited by the mean quantities, and also indicates that QGSJET and VENUS are the preferred hadronic interaction models. We find that an initially mixed composition turns lighter between 1 and 3 PeV, and then becomes heavier with increasing energy above 3 PeV.

Key words: PACS 95.85.R. Cosmic rays, Knee, Energy spectrum, Composition, Cherenkov.

[1] Corresponding author. Current address: Dept. of Physics, Princeton University,

1 Introduction

The all-particle energy spectrum of cosmic rays can be described by a steeply falling power law over many decades of energy. The smoothness of this drop in intensity with energy is broken by a change in index of the power law just above 10^{15} eV. While the origin of this break (referred to as the "knee") is not yet fully understood, the prevailing theoretical models describe the knee as a result of the energy limit for particle acceleration in supernova shocks [1]. Further, these models predict that the composition of the primary cosmic rays should change from proton (or "light"-nuclei) dominated to iron (or "heavy"-nuclei) dominated as energy increases through the region of the knee. Measuring a composition trend from light to heavy would lend support to the supernova shock acceleration picture.

Determining the composition of cosmic rays with energies greater than 10^{15} eV is a notoriously difficult problem. To detect primary cosmic rays above this energy directly by satellite experiments requires an unacceptable launch payload volume. Similarly, stratospheric balloon-borne experiments are limited by volume and flight time in their collection of primary particles. Thus, to investigate the composition of cosmic rays at the knee, we must rely on ground-based detection of air showers generated by the primary cosmic rays.

The Cherenkov light emission from the charged particle component of an air shower provides an integrated measurement of the longitudinal development [2,3]. One approach is to sample the Cherenkov lateral distribution, the photon density as a function of distance from the air shower core. The Cherenkov intensity is proportional to the primary energy, while the slope of the lateral distribution is related to the depth of maximum shower development — and hence to the mass of the primary cosmic ray nucleus. Therefore measuring a large number of Cherenkov lateral distributions can provide information on how the composition changes with energy. Previous attempts to exploit this fact at the knee include [4–6].

Optical photons suffer little absorption as they travel through the atmosphere. This means that the Cherenkov lateral distribution is much broader than that of charged particles. Additionally their numerical density is much higher. Thus it is possible to make high signal-to-noise measurements of Cherenkov lateral distributions using an array of detectors with smaller area and wider spacing than would be required for equivalent measurements of charged particles.

To obtain high quality Cherenkov lateral distribution data the Broad Lateral Non-imaging Cherenkov Array (BLANCA) was built at the Chicago Air Shower Array (CASA) installation in Dugway, Utah. Using CASA as the cos-

Princeton, New Jersey 08544, USA.

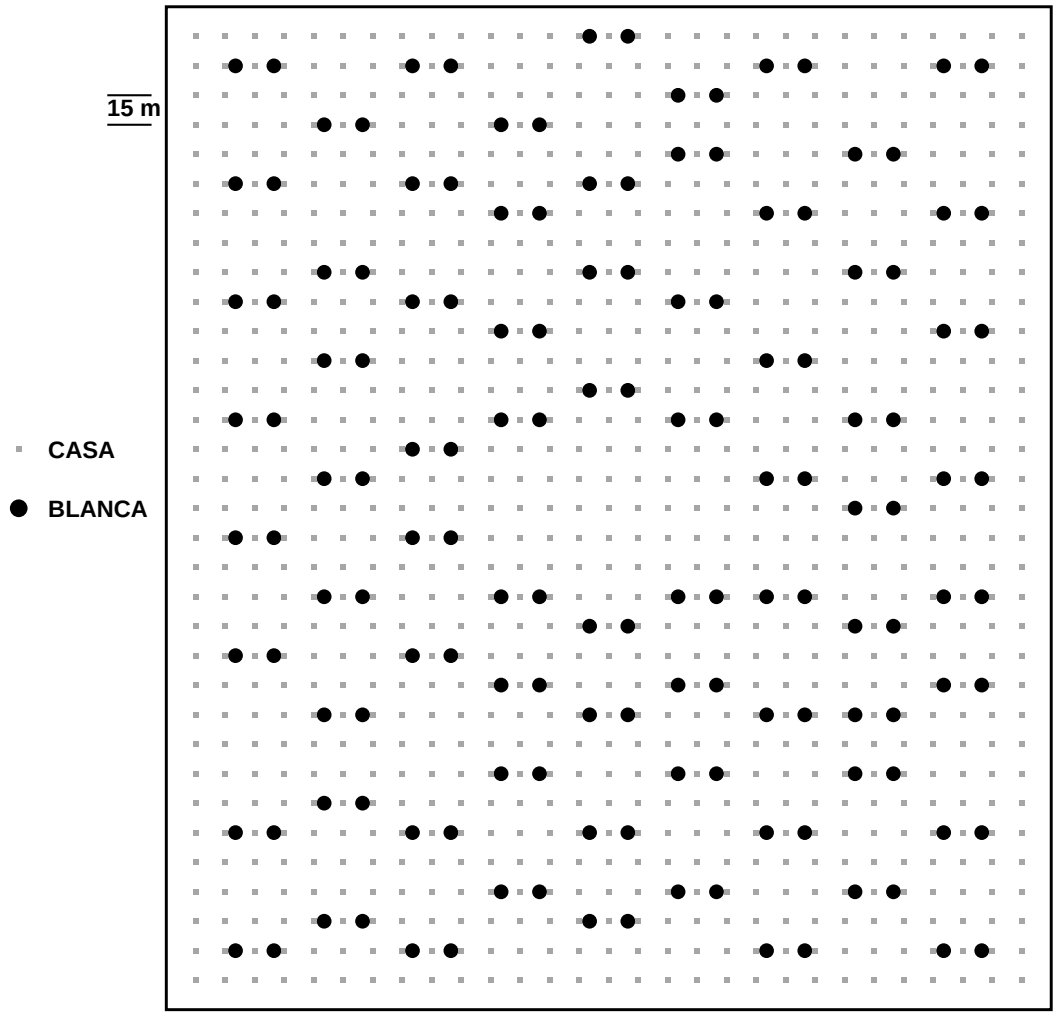

Fig. 1. The CASA-BLANCA arrays. The CASA scintillator stations were placed at 15 m intervals. The 144 BLANCA air Cherenkov detectors filled the array with characteristic separations of 35–40 m.

mic ray trigger, BLANCA operated on clear, moonless nights in 1997 and 1998. In the following analysis we use CASA to find the shower core position and arrival direction and BLANCA to make a precision measurement of the Cherenkov lateral distribution. This paper details the results obtained through these measurements on the energy spectrum and composition of cosmic rays in the energy range between 3×10^{14} and 3×10^{16} eV.

2 The CASA-BLANCA Instrument

The CASA-BLANCA instrument was located at the Dugway Proving Ground near Salt Lake City, Utah, USA, under a mean atmospheric overburden of $870\,\mathrm{g\,cm^{-2}}$. During BLANCA runs, CASA [7] consisted of 957 scintillation

counters which detected the charged particles in an air shower. The surface array covered approximately $0.2\,\mathrm{km}^2$. BLANCA [8] consisted of 144 angle-integrating detectors which recorded the lateral distribution of air shower Cherenkov light. The BLANCA detectors were not uniformly spaced but had an average separation of 35–40 m. MIA, an array of buried muon detectors at the same site, was not used in this analysis. Figure 1 shows the site plan.

Each BLANCA detector contained a large Winston cone [9] which concentrated the light striking an $800\,\mathrm{cm}^2$ entrance aperture onto a $46\,\mathrm{cm}^2$ photomultiplier. The concentrator had a nominal half-angle of 12.5° and truncated length of 60 cm. Lab measurements and simulations show that the effective half-angle was actually $\sim 10°$ because of a 6 mm gap between the photomultiplier and the cone. The Winston cones were aligned vertically with $\sim 0.5°$ accuracy. A two-output preamplifier increased the dynamic range of the detector. A typical BLANCA unit had a detection threshold of approximately one blue photon per cm^2.

The Cherenkov array did not have a separate trigger system, relying instead on triggers from CASA. Cherenkov data were recorded for all stations which exceeded a fixed threshold in coincidence with a surface array trigger. For showers in the BLANCA field of view, the CASA trigger threshold imposes a minimum energy of $\sim 100\,\mathrm{TeV}$ on the Cherenkov array. In this analysis, we use only showers with an energy of at least 200 TeV as determined by BLANCA.

3 Data Collection and Calibration

CASA-BLANCA operated on 90 moonless nights between January, 1997 and May, 1998. After removing periods of hazy or cloudy weather, approximately 460 hours of Cherenkov observations remain. Data cuts require events to have at least five good Cherenkov measurements from BLANCA and a reconstructed primary direction within 9° of zenith. Events are also cut if the core location reconstructed by CASA is outside the array or within 30 m of the edge, because core location uncertainty increases towards the edge. The geometrical and temporal cuts result in an exposure to cosmic rays of $1.83 \times 10^{10}\,\mathrm{m}^2\,\mathrm{sr}\,\mathrm{s}$.

For each night of data the BLANCA detectors are intercalibrated using the cosmic ray data itself to find their relative sensitivity to Cherenkov light. The intercalibration method depends on the circular symmetry of the Cherenkov light pool about the shower axis. Two detectors equidistant from a shower core receive, on average, equal Cherenkov photon densities, and any discrepancies can be attributed to different detector sensitivities. By averaging over suitable events in a run, we find the sensitivity ratio of each possible pair of BLANCA detectors. A maximum-likelihood method is then used to determine the set of

143 relative gains that best reproduces the pairwise ratios [10]. The reliability of this method was verified with an *in situ* intercalibration using a portable stable blue LED flasher ($\lambda \sim 430\,\mathrm{nm}$). The relative detector sensitivities are distributed log-normally with typical RMS of 0.4 in natural log.

The BLANCA absolute calibration also used the blue LED system as a reference source. The LED flasher was calibrated by using it to produce single photoelectrons in a photomultiplier with good charge resolution. Two BLANCA detectors were then calibrated in a dark box using the reference LED. The absolute calibration has a 20% systematic uncertainty, resulting mainly from the uncertain quantum efficiency of the reference photomultiplier. This absolute calibration error produces a similar uncertainty in the overall energy scale. The spectral response of the BLANCA photomultipliers was measured by the manufacturer for four representative tubes, and the relative response was assumed to be the same for all detectors.

4 Air Shower Simulations

The CASA-BLANCA analysis compares the Cherenkov measurements with air showers simulated by the CORSIKA Monte Carlo version 5.621 [11]. We used the EGS4 and GHEISHA codes for the electromagnetic and low-energy nuclear interactions. Nucleus-nucleus interactions at air shower energies are well beyond the reach of accelerator experiments. Therefore we are forced to rely on hadronic interaction models which attempt to extrapolate from the available data using different mixtures of theory and phenomenology. Several groups produce such models — in this paper we have used four: QGSJET [12], VENUS [13], SIBYLL [14], and HDPM [11]. BLANCA data are interpreted according to each model, indicating the systematic errors that depend on the choice of interaction model.

Simulated showers were produced for proton, helium, nitrogen, and iron primaries in equal numbers. Nitrogen was chosen to represent the entire CNO group. The shower libraries consist of 10,000 showers per primary species, per hadronic model. Primary energies are distributed uniformly in $\log(E)$ between 10^{14} and $10^{16.5}\,\mathrm{eV}$. Shower directions are uniform in solid angle to a maximum zenith angle of 12°. To produce such large simulated air shower libraries, it was necessary to employ the CORSIKA thinning option, which tracks only a representative sample of shower particles below a threshold energy. In all simulations, this threshold was 10^{-4} times the primary energy. Studies of simulated 1 PeV showers showed that at this thinning level, the distributions of gross properties such as the depth of shower maximum and Cherenkov slope and intensity were indistinguishable from those of unthinned showers [15].

Shower development and Cherenkov emission were simulated in Monte Carlo assuming the U. S. standard atmosphere. The CORSIKA program was modified to include a complete model of atmospheric scattering, both Rayleigh (molecular) and Mie (aerosol). Although the modified CORSIKA tracks scattered photons, few reach the ground within the BLANCA field of view, effectively making scattering an absorption process for Cherenkov photons. The scattering losses were generally similar in magnitude to the expected measurement errors and were correlated with the depth of shower maximum. Therefore, atmospheric scattering must not be ignored in analyzing the BLANCA data. On average, scattering reduces the Cherenkov intensity by $\sim 20\%$ and increases the inner slope by $\sim 7\%$. Scattering effects are smallest for late developing showers. Possible molecular absorption by oxygen and ozone was determined to be small compared with the systematic error in the absolute detector calibration and was consequently ignored.

The CORSIKA air showers were processed by a full BLANCA detector simulation which includes the measured wavelength dependence and angular response of the BLANCA detectors. Other simulated effects include detector alignment; unequal detector gains and saturation levels; night sky background light; photomultiplier response; and errors in the CASA core location and shower direction. The detector simulation produces "fake data" which is calibrated and fit like the real data. We have used this fake data to find the optimum transfer functions for converting Cherenkov measurements to air shower and primary cosmic ray parameters throughout this paper.

5 The Cosmic Ray Energy Spectrum

For each air shower event, raw BLANCA data are converted to photon densities, producing a Cherenkov lateral distribution. We fit this lateral distribution with an empirically motivated function which matches both the real and simulated data. The function is exponential in the range 30 m–120 m from the shower core and a power law from 120 m–350 m. It has three parameters: a normalization C_{120}, the exponential "inner slope" s, and the power law index β:

$$C(r) = \begin{cases} C_{120}\ e^{s(120\,\mathrm{m}-r)}, & 30\,\mathrm{m} < r \le 120\,\mathrm{m} \\ C_{120}\ (r/120\,\mathrm{m})^{-\beta}, & 120\,\mathrm{m} < r \le 350\,\mathrm{m} \end{cases} \quad (1)$$

The energy of each air shower is derived using only the C_{120} and s parameters of the Cherenkov lateral distribution fit. The outer slope β is not used, both because it correlates strongly with s and because it is subject to larger mea-

surement errors. The Monte Carlo fake data libraries (including detector simulation) are used to determine the relationship between measured quantities and energy. The energy depends primarily on C_{120}, the Cherenkov intensity 120 m from the core. We fit the logarithm of the energy as a quadratic function of $\log C_{120}$ (the curvature is small, typically 0.005 decades^{-1}). In all hadronic models, C_{120} grows approximately as $E^{1.07}$, because the fraction of primary energy directed into the electromagnetic component of the cascade increases with energy.

According to the Monte Carlo, the quadratic function used to estimate the energy works well for most showers but has a bias such that energies are slightly underestimated for showers with unusually large or small depths of maximum development. Therefore, a small correction is applied to the energy estimate. The correction depends on the Cherenkov slope s and on the shower zenith angle. The magnitude of this energy correction is less than 10% for 85% of BLANCA showers.

Energies derived from the data in this manner have an error distribution which depends on the primary mass and energy. In general, the random errors on reconstructing a single shower's energy are comparable to the systematic uncertainty due to the unknown composition. Assuming a mixed cosmic ray composition, the BLANCA energy resolution for a single air shower is approximately 12% for a 200 TeV shower, falling to 8% for energies above 5 PeV.

The differential all-particle cosmic ray flux measured by CASA-BLANCA is shown in Figure 2, scaled up by a factor of $(E/1\,\mathrm{GeV})^{2.75}$ to emphasize the structure. Table A.1 lists the values of the observed spectrum. The energy spectrum is compared with that reported by several other groups. Although the CASA-BLANCA, DICE, and CASA-MIA experiments shared some instrumentation, their data sets and energy analysis methods are entirely independent. These three experiments show very good agreement in their spectrum determination. Most other results are consistent with CASA-BLANCA, given the 20% or larger energy systematic error typical of air shower measurements.

The spectrum shown in Figure 2 uses event energies derived from the Cherenkov predictions of CORSIKA with the QGSJET hadronic interaction model. The data can also be interpreted using the other available interaction models. The alternate energy estimates lead to spectra with no qualitatively different features. Instead, they amount only to a shift in energy scale of order 10%, less than the BLANCA instrumental energy scale uncertainty. HDPM and VENUS predict less Cherenkov light and hence assign higher energies than QGSJET does, while the SIBYLL simulations lead to lower assigned energies.

Figure 2 contains the knee region of the spectrum, near 3 PeV. The CASA-BLANCA spectrum exhibits a smooth change rather than a sharp break here.

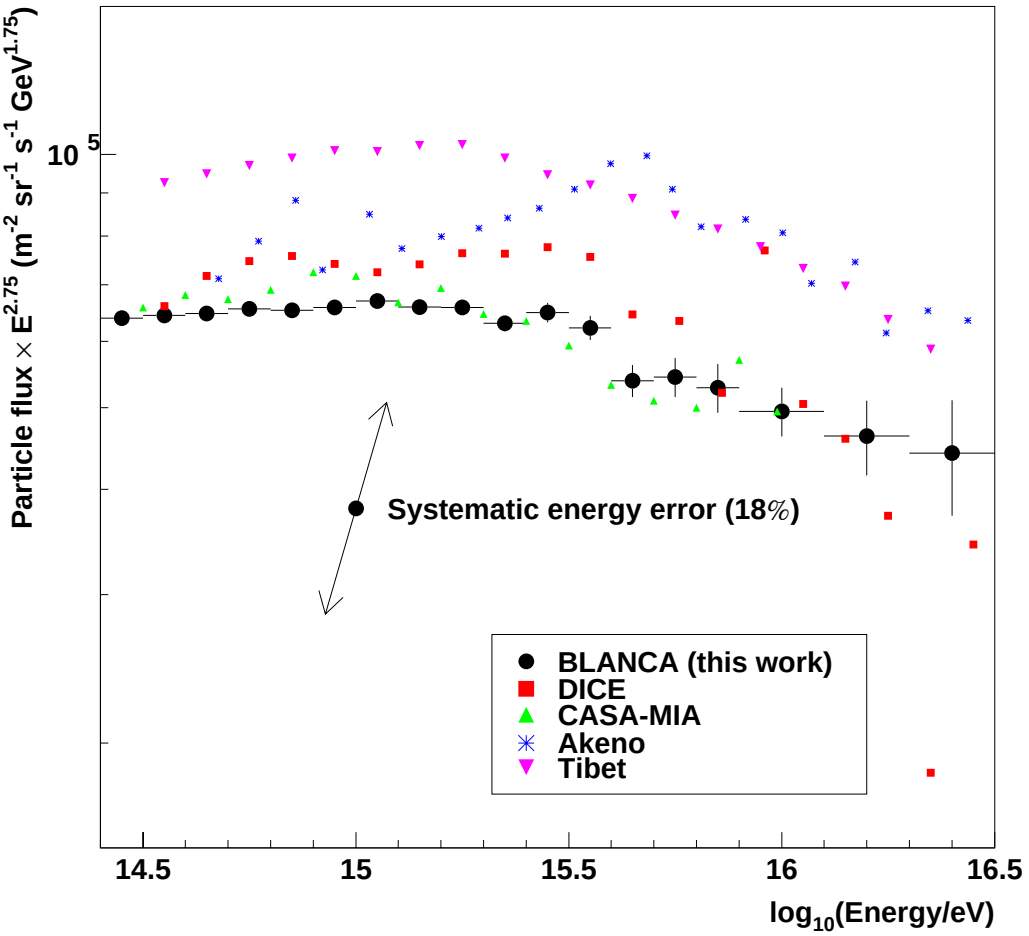

Fig. 2. The differential all-particle cosmic ray flux measured by CASA-BLANCA (QGSJET energy). Each data point represents the differential flux scaled up by a factor of $(E/1\,\mathrm{GeV})^{2.75}$; the error bars represent statistical (Poisson) errors only. The diagonal bar shows the effect of a possible systematic energy shift of $\pm 18\%$. Also plotted are the cosmic ray fluxes reported by DICE [16], CASA-MIA [17], Akeno [18] and Tibet ASγ [19].

However, measurements over a wider energy range show that the form of the cosmic ray spectrum is a power law well above and below 3 PeV. Historically, many groups have found the knee to be quite sharp. In the spirit of the usual discussion of the knee, we have fit several similar functions to the data (Figure 3, top). The fits find simultaneously the position (energy) of the knee and the power law indices above and below the knee. A log-likelihood fit is performed in order to account for the Poisson statistics of discrete events in a binned energy distribution.

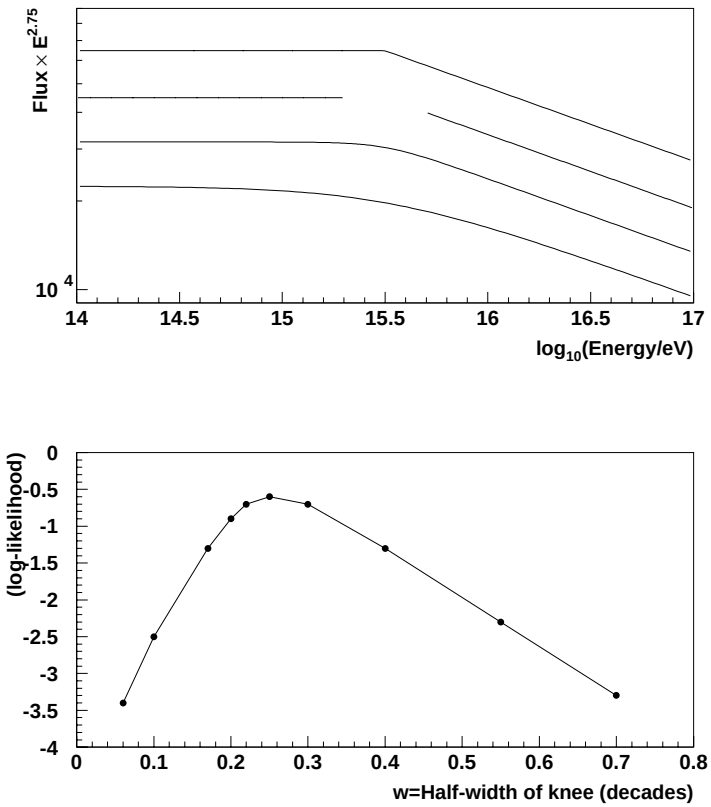

Fig. 3. *Top:* Several trial functions used to fit the cosmic ray flux. *Bottom:* The log-likelihood for the smooth function at a range of widths w. The CASA-BLANCA data fit best to a knee with $w = 0.25$, or a full width of one-half decade.

Of the trial functions, the smoothly changing power law fits the BLANCA data best:

$$J(E) = J_k \left(\frac{E}{E_k}\right)^{\alpha} \left[1 + \left(\frac{E}{E_k}\right)^{\frac{1}{w}}\right]^{(\beta-\alpha)w} \tag{2}$$

E_k is the energy at the center of the transition, *i.e.* the knee energy. For $E \ll E_k$, the function is a power law with index α, while the spectral index becomes β for $E \gg E_k$. Parameter J_k sets the normalization at the knee. The fifth parameter, w, is the half-width in decades of the transition region. The lower panel of Figure 3 shows how the log-likelihood depends on the choice of w. The data favor a knee one-half decade wide ($w = 0.25$). The best-fit knee energy is $2.0^{+0.4}_{-0.2}$ PeV, with power law indices of $\alpha = -2.72 \pm 0.02$ and $\beta = -2.95 \pm 0.02$. Figure 4 shows the energy spectrum near the knee using fine bins 0.04 decades wide as well as the best fit curve.

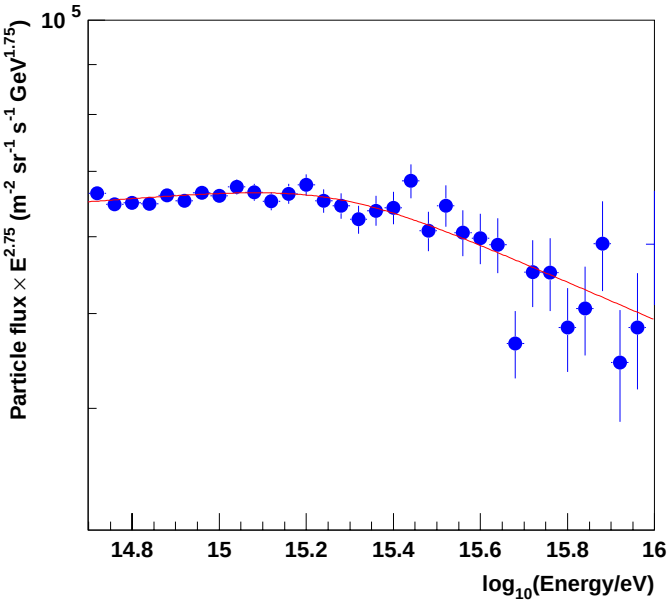

Fig. 4. The CASA-BLANCA energy spectrum shown with more detail in the knee region.

6 Depth of Shower Maximum

The depth of shower maximum (X_{max}) is an important characteristic of air shower development which, for given energy, is related to the mass of the primary particle. However, like all air shower parameters, the relationship depends on the choice of uncertain high energy hadronic interaction model parameters. Imaging experiments such as Fly's Eye [20], and to a lesser extent DICE [16], measure X_{max} rather directly. The importance of X_{max} for various other types of ground-based experiment has long been known [21]; measured parameters can often be translated into the depth of shower maximum in a way which is rather independent of the hadronic model. Therefore X_{max} provides a useful middle ground on which experiments may publish and compare their results.

The mean X_{max} for a given primary type grows logarithmically with energy at an approximate elongation rate of $80\,\mathrm{g\,cm^{-2}}$ per decade, although this value depends on the hadronic model used. The expected X_{max} is similar for two primaries of different mass if they have equal energy per nucleon.

To determine the optimum transfer function for converting Cherenkov lateral distributions into X_{max}, we study the same set of simulated showers used to derive the primary energy function. The fake data libraries use the four

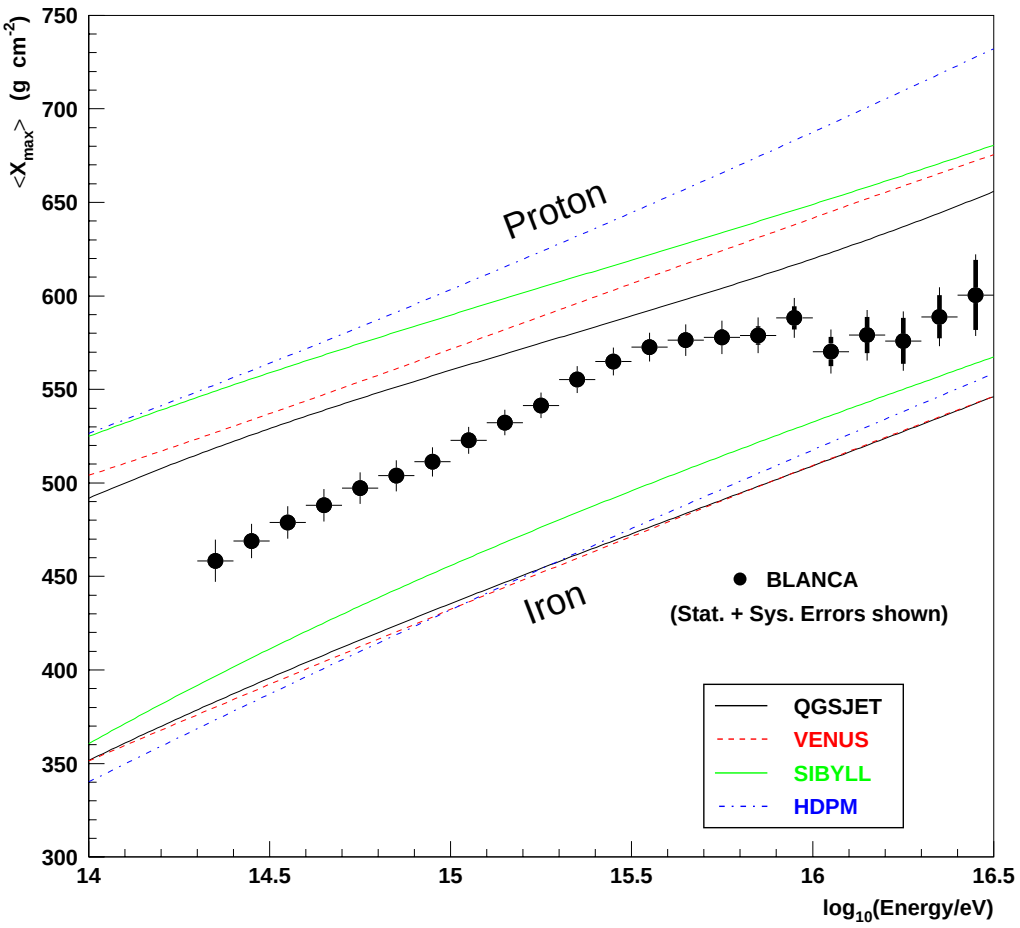

Fig. 5. The mean depth of shower maximum $\langle X_{max} \rangle$ measured by CASA-BLANCA as a function of energy. The lines represent the values for pure proton or pure iron samples predicted by each of the four hadronic interaction models. The thick error bars represent the statistical uncertainty, while the thin errors also include the systematic uncertainties discussed in the text; the former are important only above 10 PeV.

primary types and four hadronic interaction models processed through the BLANCA detector simulation. The simulated Cherenkov lateral distributions are fit to the function in Equation 1, which is exponential with a slope s from 30 m to 120 m from the core. The combined shower and detector simulations show that this inner slope is linearly related to X_{max} except for the deepest developing showers; an additional small quadratic term is required for slopes exceeding $s_\star = 0.018\,\mathrm{m}^{-1}$.

The mean X_{max} is shown in Figure 5 as a function of energy. Both quantities are derived from the CASA-BLANCA data using the CORSIKA/QGSJET Monte Carlo results. We indeed find that the results are very similar if any

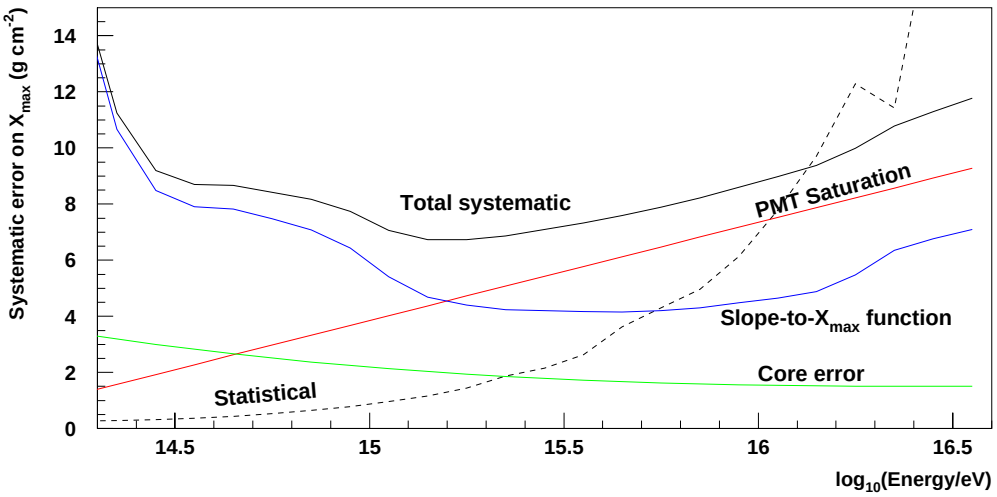

Fig. 6. Systematic uncertainties on CASA-BLANCA X_{max} estimates. At low energies, the dominant error comes from the slope-to-X_{max} conversion function; at high energies, the uncertain photomultiplier linearity is more important. For comparison, the statistical error on the CASA-BLANCA mean X_{max} measurements is also shown (dashed line), assuming a bin width of 0.1 decades.

of the other hadronic models are used instead. Numerical results are given in Table A.2. Figure 5 also shows the mean X_{max} expected for pure samples of proton primaries and iron primaries. SIBYLL generally predicts deeper shower maximum than other models, while HDPM exhibits a steeper elongation rate than the others ($\sim 90\,\mathrm{g\,cm^{-2}}$ per decade compared with 70–75 $\mathrm{g\,cm^{-2}}$ typical of the other models). The BLANCA results are clearly consistent with a mixed composition throughout the energy range, regardless of the preferred hadronic model. The data suggest that the composition becomes lighter approaching the knee and then becomes heavier at higher energies.

The shower depth estimated from Cherenkov observations is subject to a number of small systematic uncertainties. Random core errors lead to a systematic flattening of the Cherenkov inner slope, but the effect is only a very small bias toward deeper X_{max}. Photomultiplier saturation poses a potential problem at high energies. However, the nonlinearity has been characterized in laboratory studies of fourteen BLANCA detectors and the data corrected for its effects. The uncertainty on this correction leads to a systematic error in X_{max} which is only $10\,\mathrm{g\,cm^{-2}}$ at the highest energies. A third error dominates at energies below 1 PeV. This error arises from the limitations of the function which converts Cherenkov slope to an estimate of X_{max}. The function tends to overestimate the depth of showers at the extreme ends of the BLANCA energy range. It is difficult to overcome this weakness without introducing at the same time

a much larger bias which depends on X_{max} itself. Instead, we take the error found in Monte Carlo studies as a systematic error on the measured X_{max}. The independent errors are added in quadrature to find the total systematic error (Figure 6). Systematic errors are important only below 10 PeV. At high energy, statistical errors are the more serious limitation on measuring mean X_{max}.

7 Mean Nuclear Mass

The mean depth of shower maximum results presented above are essentially independent of a particular hadronic interaction model. They are therefore useful for comparison with other experiments and re-interpretation on the basis of future hadronic interaction models. However, a quantity which is of much more direct astrophysical interest is the mean nuclear mass of the primary cosmic rays.

We choose to derive mean primary mass directly from the Cherenkov lateral distribution slope s. It would make little difference if we were to do so via the X_{max} values discussed in the previous section. The important point is that while the transfer function from s to X_{max} is rather independent of the hadronic interaction model, any interpretation in terms of absolute nuclear mass is not. This is clear from the disparity among the models of the mean proton and iron X_{max} values shown in Figure 5.

At fixed primary energy, s and X_{max} both depend linearly on the logarithm of nuclear mass A, as do most composition-sensitive air shower parameters. Following previous authors, we choose to work with the natural log, $\ln(A)$. Unlike $X_{max}=f_1(s)$, the transfer function $\ln(A)=f_2(s)$ depends on energy. Therefore we divide the Monte Carlo fake data into six bands of C_{120} and perform a linear fit to $\ln(A)$ versus s in each. To interpret each real event the slope and intercept of the transfer function are interpolated between the appropriate bracketing bands.

This method has little systematic bias apart from the differences between hadronic interaction models. The mean reconstructed $\ln(A)$ for a pure sample of each simulated primary species is accurate to to $\pm 20\%$ over the BLANCA energy range. On the other hand, the random error is large on any single measurement of $\ln(A)$. Shower-by-shower estimates of primary mass cannot be made with any accuracy — the fluctuations inherent in the air shower process preclude them. Nevertheless, the mean value of $\ln(A)$ provides a useful indicator of the cosmic ray mass composition.

The mean $\ln(A)$ is shown as a function of primary energy in Figure 7. The four

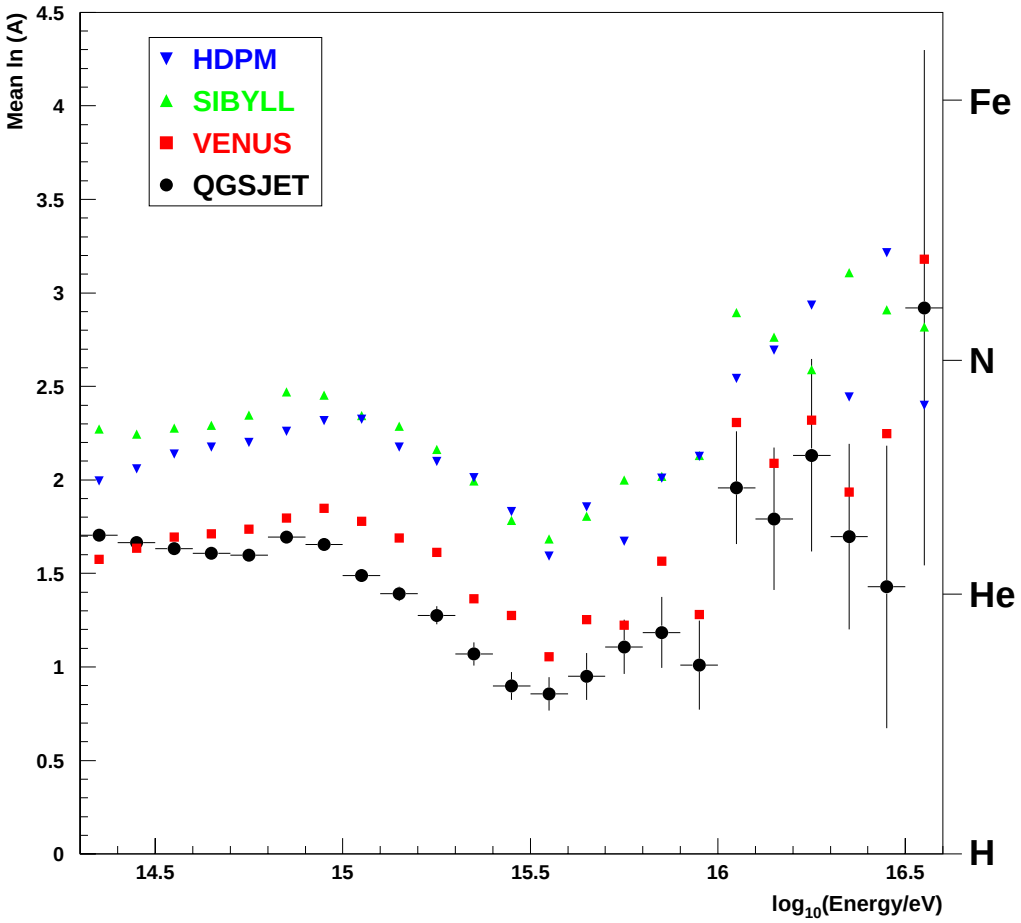

Fig. 7. The mean logarithmic mass $\langle \ln(A) \rangle$ measured by CASA-BLANCA as a function of energy. The four sets of symbols show the BLANCA data interpreted using CORSIKA coupled with the indicated hadronic interaction model. Error bars are statistical only and shown only on the QGSJET results; errors on the other points are of similar size. Assuming a hadronic model, the systematic uncertainties in the $\ln(A)$ estimate are typically 0.2. The dominant systematic effect is clearly the difference *between* the hadronic models.

sets of symbols show the BLANCA data interpreted using CORSIKA coupled with each of the hadronic codes. Numerical results are given in Table A.3. The dependence on interaction model is clear: the models set the overall mass scale differently, but they indicate the same mass variation with energy. The mean mass becomes lighter with increasing energy through the knee, then becomes heavier above $\sim 3\,\mathrm{PeV}$. The $\ln(A)$ plot exhibits the same trends seen in the X_{max} results of the previous section.

8 A Multi-species Fit to the Cherenkov Data

The techniques described above involve estimating X_{max} or $\ln(A)$ for each shower and then taking the *average* over all showers in a given energy range. By considering only the average value we lose much of the available information. Instead the measured distribution of a composition sensitive parameter can be compared with those predicted for a number of simulated primary species, providing a more powerful technique to study cosmic ray composition.

Comparing measured and simulated distributions requires high statistics samples for both the real and Monte Carlo data sets. We separate the data into five logarithmic energy bins between $10^{14.5}$ and $10^{16.5}$ eV. This bin choice is a compromise between the need to include many showers in each range and the wish to examine trends on as fine an energy scale as possible. Within each range, we find the distribution of the Cherenkov inner slope (s) for the real data and for pure samples of each species in the Monte Carlo library (protons, He, N, and Fe). The simulated distributions of s (with detector effects) are smoothed by a multiquadric smoothing algorithm [22]. To preserve information about their limited statistics, the data distributions are not smoothed.

The multi-species fit in each energy range finds the linear combination of the four simulated distributions which reproduces the data distribution best. Since each primary species has a characteristic shape of its s distribution, this fit uses more information than simply the mean or even the width of s. We do not *a priori* require the fractional contribution of each primary type to lie in the physical range of 0–100%, nor is the sum of the fractions constrained to equal 1.0. In practice, however, the sum is always in the range $100 \pm 0.5\%$. The fits use a MINUIT-based log-likelihood maximization procedure [23], which accounts properly for the Poisson probability distribution of data events in bins with low statistics.

As an example, Figure 8 shows the multi-species fit in the energy range $10^{14.9}$–$10^{15.3}$ eV. The lower right panel (#4) displays the full fit using all four available primary types. The other panels show the best fits that can be made when helium (#2), nitrogen (#3), or both (#1) are omitted. The Monte Carlo predictions cannot match the data using protons and iron alone; the intermediate mass nitrogen species is also required. Panel #2 shows that the best fit of p, N, and Fe to the data is very close but fails to match the shape at the peak and in the long tail to high values of s. The data strongly suggest that at least the four primary types considered here contribute to the cosmic rays just below the knee.

The fits demonstrated in Figure 8 (lower right) are performed for all five energy ranges and using the predictions of all four high energy hadronic interaction

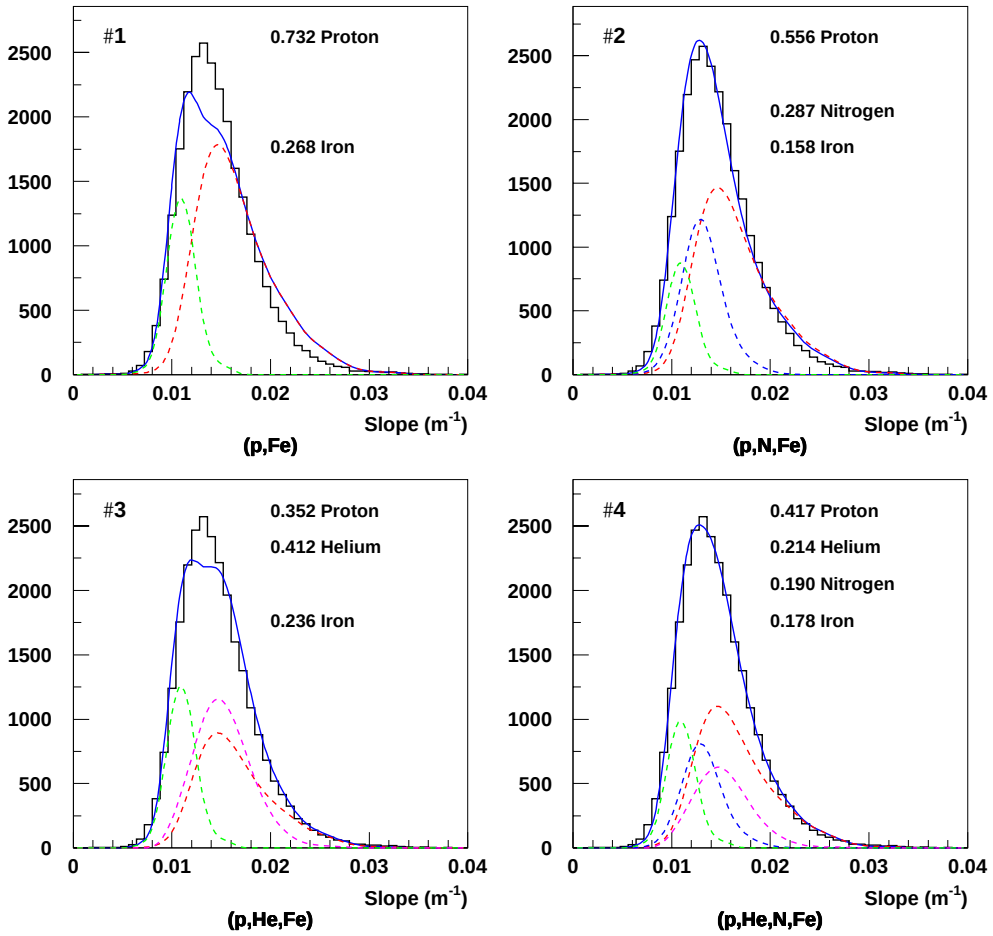

Fig. 8. A demonstration of the multi-species fitting procedure, in this case the energy range $10^{14.9} - 10^{15.3}$ eV. The solid histogram gives the distribution of Cherenkov slope s for all CASA-BLANCA data in that energy range and is the same in all four panels. The solid curves show the combinations of Monte Carlo (QGSJET) showers which best reproduce the measured distribution. Panels 1–4 correspond to different combinations of primary species. Clearly a nitrogen component is needed to match the data, but a helium component is also important.

models. Gauging the goodness of fit presents a problem. As stated above the multi species fit uses a log-likelihood maximization procedure; although this is an appropriate method for extracting abundance fractions from the binned data, the actual value of the likelihood is not useful [23]. Therefore we calculate and use the familiar $\overline{\chi}^2$ quantity as a rough guide to the fit quality. In the lowest energy range, the number of data events is so large that no combination of the four cosmic ray species can reproduce the data adequately. This is probably the result of limitations of the shower and detector simulations, although it could also be due to the limited number of species considered. Conversely, the

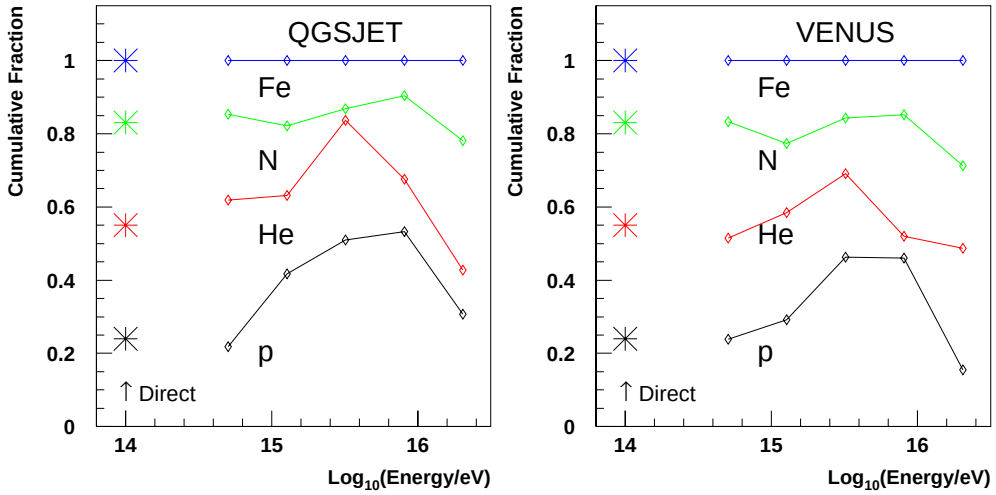

Fig. 9. Results of the multi-species fit to the CASA-BLANCA data. The line graphs indicate the mixture of proton, helium, nitrogen, and iron primaries which best reproduces the Cherenkov slope distributions of the data. The lines show *cumulative* fractions (*i.e.* the lowest line gives the proton fraction, while the next line gives the combined proton and helium fraction). QGSJET (*left*) and VENUS (*right*) are shown. The other two interaction models show similar trends but with heavier overall composition. The stars ($*$) at 10^{14} eV show the results of direct measurements from the JACEE balloon-borne emulsion experiment [24,25]. JACEE Ne-Si data have been divided evenly into the N and Fe groups for comparison with BLANCA.

high energy ranges have too few events to constrain the abundances well. The results for all models are presented in Table A.4.

The results of the multi-species fit to the BLANCA Cherenkov slope data are shown in Figure 9 for the QGSJET and VENUS models. The SIBYLL and HDPM models show similar trends but a heavier overall composition. These latter two models also give unphysical negative helium abundances in at least one energy bin, and systematically poorer fits. At 100 TeV, data from the JACEE balloon direct measurements [24,25] are shown for comparison. The direct composition at 100 TeV agrees well with the BLANCA data at 400 TeV. The results of the multi-species fit also agree with the mean X_{max} and mean $\ln(A)$ derived in the previous two sections. All three ways of interpreting the data indicate that the cosmic ray composition is lighter near 3 PeV than it is at either 300 TeV or 30 PeV.

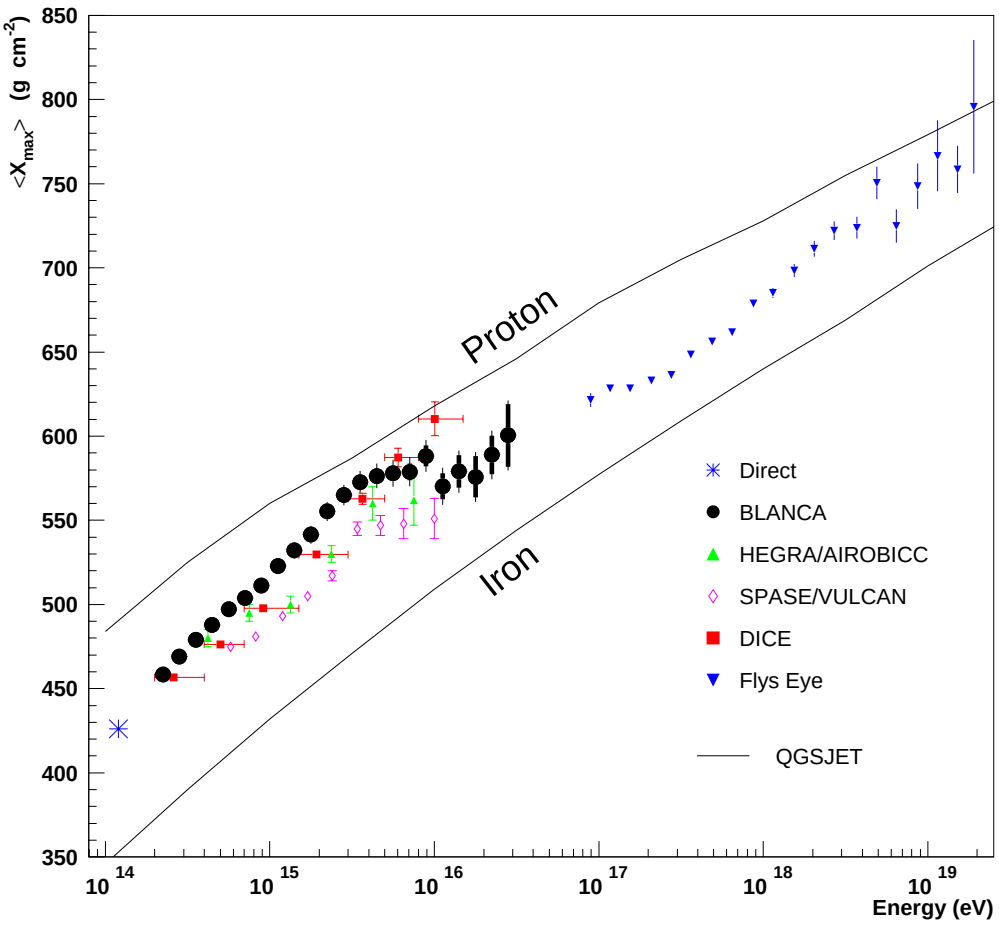

Fig. 10. The CASA-BLANCA measurement of X_{max} compared with other results. All experiments operating near the knee use atmospheric Cherenkov light, including DICE [16], the AIROBICC array of HEGRA [5], and the VULCAN array at the South Pole [6]. The high energy measurements ($> 10^{17}$ eV) by Fly's Eye use the atmospheric fluorescence technique [26]. The "direct" point estimates the mean X_{max} that would be expected on the basis of direct balloon measurements [16]. The Monte Carlo lines use CORSIKA with QGSJET [27].

9 Conclusions

The CASA-BLANCA experiment has studied cosmic rays in the energy range 0.3–30 PeV. The primary energy and mass are found by measuring the Cherenkov lateral distribution for each air shower. In an effort to understand how results depend on the unknown physics of high energy nuclear interactions, we have interpreted the data using the CORSIKA air shower Monte Carlo program with four different hadronic interaction models: QGSJET, VENUS, SIBYLL, and HDPM.

The BLANCA energy spectrum agrees well with previous measurements and exhibits a smooth knee near 2–3 PeV in primary energy. The model dependence of the energy scale is less than the absolute calibration uncertainty.

We find the transformation from measured Cherenkov lateral distribution slope to the depth of shower maximum X_{max} to be essentially model independent. In Figure 10 our results are compared to previous experiments over a wide energy range. The BLANCA data are well within the physically reasonable range bounded by the pure proton and iron curves; furthermore they are consistent at low energy with those expected from direct measurements and at high energy with the Fly's Eye result [26].

We have also interpreted our data as a mean nuclear mass. This is essentially equivalent to the X_{max} analysis but is a quantity of more direct astrophysical interest.

It has been a long held goal in the air shower field to choose an adequate hadronic interaction model *and* determine the nuclear composition of the primary cosmic rays simultaneously. With the advent of the powerful simulation tool provided by the CORSIKA group, and high collecting power arrays such as CASA-BLANCA, it seems that this ambition may be becoming a reality. A multi component fit of the type described in Section 8 is a much more efficient use of the available data than simply considering the mean value and spread of a quantity, and the experimental statistics are starting to justify this approach. The agreement between data and simulation in Figure 8 is impressive.

On the basis of our data we favor the QGSJET and VENUS models and reject SIBYLL and HDPM. At the same time, both of the ways in which we have analyzed our data indicate that the cosmic ray composition is lighter near 3 PeV than it is at either 300 TeV or 30 PeV. The trend towards heavier primary mass above 3 PeV agrees with the canonical model of Galactic production and a rigidity-dependent time for escape, and is not consistent with acceleration at sites such as AGN, which require a pure proton composition well above the knee [28].

The trend shown in our data to a lighter composition approaching the knee is puzzling but not without theoretical precedent. Swordy, arguing that there must be a minimum path length in the Galaxy even for the highest energy cosmic rays, predicts a light composition at the knee [29].

We acknowledge the invaluable assistance of the CASA-MIA collaboration, as well as the University of Utah High-Resolution Fly's Eye (HiRes) group and the command and staff of the U.S. Army Dugway Proving Ground. We thank D. Heck and the rest of the CORSIKA team for providing and maintaining their excellent program, and the authors of the hadronic interaction models to which it is linked. We thank C. Cassidy, J. Jacobs, J. Meyer, M. Pritchard,

and K. Riley for helping with BLANCA's construction and K. Anderson and C. Eberhardy for calibration work. We especially wish to thank M. Cassidy for his essential contributions as our technician. We would also like to thank S. Swordy for useful conversations. JF and CP acknowledge fellowships from the William Grainger Foundation and the Robert R. McCormick Foundation, respectively. This work was supported by the U.S. National Science Foundation.

A Data tables

References

[1] L. O'C. Drury *et al.*, *Astron. Astrophys.*, **287** (1994) 959.

[2] M. H. Brennan *et al.*, *Nature*, **182** (1958) 973.

[3] A. E. Chudakov *et al.*, *Proc. 6th Int. Conf. on Cosmic Rays, Moscow*, **2** (1960) 47.

[4] B. R. Dawson *et al.*, *J. Phys. G: Nucl. Part. Phys.*, **15** (1989) 893.

[5] F. Arqueros *et al.*, accepted in Astron. Astrophys. (1999). Preprint astro-ph/9908202.

[6] J. E. Dickinson *et al.*, *Proc. 26th Int. Cosmic Ray Conf., Salt Lake City*, **3**, 136 (1999).

[7] A. Borione *et al.*, Nucl. Instrum. Meth., **A346**, 329 (1994).

[8] M. Cassidy *et al.*, *Proc. 25th Int. Cosmic Ray Conf., Durban*, **5** , 189 (1997).

[9] W. T. Welford and R. Winston, *High Collection Non-imaging Optics*, Academic Press, San Diego, 1989.

[10] J. W. Fowler, PhD Thesis, University of Chicago, 2000.

[11] D. Heck *et al.*, Report FZKA 6019, Institut für Kernphysik, Forschungszentrum Karlsruhe, 1998.

[12] N. N. Kalmykov, S. S. Ostapchenko, and A. I. Pavlov, Bull. Russ. Acad. Sci. (Physics), **58**, 1966 (1994).

[13] K. Werner, Phys. Reports, **232**, 87 (1993).

[14] R. S. Fletcher *et al.*, Phys. Rev. D, **50**, 5710 (1994).

[15] L. F. Fortson *et al.*, *Proc. 26th Int. Cosmic Ray Conf., Salt Lake City*, **5**, 336 (1999).

[16] S. P. Swordy and D. B. Kieda, preprint astro-ph/9909381, accepted in *Astroparticle Phys.*, 1999.

[17] M. A. K. Glasmacher, *et al.*, Astroparticle Phys., **10**, 291 (1999).

[18] M. Nagano *et al.*, J. Phys. G, **10**, 1295 (1984).

[19] M. Amenomori *et al.*, Astrophys. J., **461**, 408 (1996).

[20] R. M. Baltrusaitis *et al.*, Nucl. Instr. and Meth. A **240**, 410 (1985).

[21] J. R. Patterson and A. M. Hillas, J. Phys. G, **9**, 1433 (1983).

[22] F. James, "HBOOK Reference Manual, Version 4.24," CERN Program Library Long Writeup Y250, Geneva, 1995.

[23] F. James, "MINUIT Reference Manual," CERN Program Library Long Writeup D506, Geneva, 1994.

[24] M. L. Cherry *et al.*, *Proc. 25th Int. Cosmic Ray Conf., Durban*, **4**, 1 (1997).

[25] A. A. Watson, *Proc. 25th Int. Cosmic Ray Conf., Durban*, **8**, 257 (1997).

[26] D. Bird *et al.*, Phys. Rev. Lett., **71**, 3401 (1993).

[27] C. Pryke, "Shower Model Comparison I: Longitudinal Profile," Pierre Auger project technical note GAP-98-035, FNAL, 1998.

[28] R. J. Protheroe and A. P. Szabo, Phys. Rev. Lett., **69**, 2885 (1992).

[29] S. Swordy, *Proc. 24th Int. Cosmic Ray Conf., Rome*, **2**, 697 (1995).

Energy range	Differential flux $J(E)$ in each bin
$\log_{10}(E/1\,\mathrm{eV})$	$(\mathrm{m}^{-2}\,\mathrm{sr}^{-1}\,\mathrm{s}^{-1}\,\mathrm{GeV}^{-1})$
14.3 – 14.4	$(12.12 \pm 0.04) \times 10^{-11}$
14.4 – 14.5	$(6.68 \pm 0.02) \times 10^{-11}$
14.5 – 14.6	$(3.58 \pm 0.02) \times 10^{-11}$
14.6 – 14.7	$(1.91 \pm 0.01) \times 10^{-11}$
14.7 – 14.8	$(1.03 \pm 0.01) \times 10^{-11}$
14.8 – 14.9	$(5.42 \pm 0.04) \times 10^{-12}$
14.9 – 15.0	$(2.90 \pm 0.03) \times 10^{-12}$
15.0 – 15.1	$(1.57 \pm 0.02) \times 10^{-12}$
15.1 – 15.2	$(8.18 \pm 0.12) \times 10^{-13}$
15.2 – 15.3	$(4.36 \pm 0.08) \times 10^{-13}$
15.3 – 15.4	$(2.21 \pm 0.05) \times 10^{-13}$
15.4 – 15.5	$(1.22 \pm 0.03) \times 10^{-13}$
15.5 – 15.6	$(6.2 \pm 0.2) \times 10^{-14}$
15.6 – 15.7	$(2.9 \pm 0.1) \times 10^{-14}$
15.7 – 15.8	$(1.5 \pm 0.1) \times 10^{-14}$
15.8 – 15.9	$(7.7 \pm 0.5) \times 10^{-15}$
15.9 – 16.1	$(2.9 \pm 0.2) \times 10^{-15}$
16.1 – 16.3	$(8.1 \pm 0.8) \times 10^{-16}$
16.3 – 16.5	$(2.1 \pm 0.3) \times 10^{-16}$
16.5 – 16.7	$(3.1 \pm 1.0) \times 10^{-17}$
16.7 – 16.9	$(2.3 \pm 0.7) \times 10^{-17}$

Table A.1
The primary cosmic ray energy spectrum measured by CASA-BLANCA. Bin widths rise with increasing energy so that $E_{max}/E_{min} = 10^{0.1}$ at lower energies, while $E_{max}/E_{min} = 10^{0.2}$ for the five highest bins. Errors represent only the Poisson uncertainty in each bin. There is an additional instrumental systematic uncertainty of 18%. These results use the QGSJET-derived energy transfer function.

Energy range $\log_{10}(E/\,\mathrm{eV})$	Mean s $(10^{-3}\,\mathrm{m}^{-1})$	$\langle X_{max}\rangle \pm$ stat. $\pm$ sys. $(\,\mathrm{g\,cm}^{-2})$
14.3 – 14.4	11.4 ± 0.0	$458 \pm 0.3 \pm 12$
14.4 – 14.5	11.9 ± 0.0	$469 \pm 0.3 \pm 10$
14.5 – 14.6	12.5 ± 0.0	$479 \pm 0.4 \pm 9$
14.6 – 14.7	12.9 ± 0.0	$488 \pm 0.4 \pm 9$
14.7 – 14.8	13.4 ± 0.0	$497 \pm 0.5 \pm 9$
14.8 – 14.9	13.7 ± 0.0	$504 \pm 0.6 \pm 9$
14.9 – 15.0	14.1 ± 0.0	$511 \pm 0.8 \pm 8$
15.0 – 15.1	14.7 ± 0.0	$523 \pm 1 \pm 7$
15.1 – 15.2	15.2 ± 0.1	$532 \pm 1 \pm 7$
15.2 – 15.3	15.6 ± 0.1	$542 \pm 1 \pm 7$
15.3 – 15.4	16.3 ± 0.1	$555 \pm 2 \pm 7$
15.4 – 15.5	16.8 ± 0.1	$565 \pm 2 \pm 7$
15.5 – 15.6	17.2 ± 0.1	$573 \pm 3 \pm 7$
15.6 – 15.7	17.3 ± 0.2	$576 \pm 4 \pm 8$
15.7 – 15.8	17.4 ± 0.2	$578 \pm 4 \pm 8$
15.8 – 15.9	17.5 ± 0.2	$579 \pm 5 \pm 8$
15.9 – 16.0	17.9 ± 0.3	$588 \pm 6 \pm 9$
16.0 – 16.1	17.0 ± 0.4	$570 \pm 8 \pm 9$
16.1 – 16.2	17.5 ± 0.4	$579 \pm 10 \pm 9$
16.2 – 16.3	17.4 ± 0.6	$576 \pm 12 \pm 10$
16.3 – 16.4	18.1 ± 0.5	$589 \pm 11 \pm 11$
16.4 – 16.5	18.5 ± 0.8	$600 \pm 19 \pm 11$
16.5 – 16.6	17.2 ± 1.5	$570 \pm 31 \pm 12$

Table A.2
The mean Cherenkov inner slope (s) measured by CASA-BLANCA and the corresponding mean X_{max}. The first column of errors given for each quantity is statistical; the standard deviation divided by $\sqrt{N}$. For X_{max} a systematic error is given which is due to a combination of effects (see Section 6). These results use the QGSJET-derived X_{max} transfer function.

Energy range	Mean ln(A)			
$\log_{10}(E/1\,\mathrm{eV})$	QGSJET	VENUS	SIBYLL	HDPM
14.3 – 14.4	1.71 ± 0.01	1.58	2.27	1.99
14.4 – 14.5	1.67 ± 0.01	1.63	2.24	2.06
14.5 – 14.6	1.63 ± 0.01	1.69	2.28	2.14
14.6 – 14.7	1.61 ± 0.01	1.71	2.29	2.18
14.7 – 14.8	1.60 ± 0.02	1.74	2.35	2.20
14.8 – 14.9	1.69 ± 0.02	1.80	2.47	2.26
14.9 – 15.0	1.65 ± 0.03	1.85	2.45	2.32
15.0 – 15.1	1.49 ± 0.03	1.78	2.34	2.32
15.1 – 15.2	1.39 ± 0.04	1.69	2.29	2.18
15.2 – 15.3	1.28 ± 0.05	1.61	2.16	2.10
15.3 – 15.4	1.07 ± 0.06	1.36	1.99	2.01
15.4 – 15.5	0.90 ± 0.07	1.28	1.78	1.83
15.5 – 15.6	0.86 ± 0.09	1.06	1.68	1.59
15.6 – 15.7	0.95 ± 0.12	1.25	1.81	1.85
15.7 – 15.8	1.1 ± 0.1	1.2	2.0	1.7
15.8 – 15.9	1.2 ± 0.2	1.6	2.0	2.0
15.9 – 16.0	1.0 ± 0.2	1.3	2.1	2.1
16.0 – 16.1	2.0 ± 0.3	2.3	2.9	2.5
16.1 – 16.2	1.8 ± 0.4	2.1	2.8	2.7
16.2 – 16.3	2.1 ± 0.5	2.3	2.6	2.9
16.3 – 16.4	1.7 ± 0.5	1.9	3.1	2.4
16.4 – 16.5	1.4 ± 0.8	2.2	2.9	3.2
16.5 – 16.6	2.9 ± 1.4	3.2	2.8	2.4

Table A.3
The mean ln(A) measured by CASA-BLANCA. The four columns show the data interpreted according to each hadronic interaction model. The variation provides some insight into the systematic errors. Statistical errors shown on the QGSJET points are similar for all four models.

Energy Range	..... Abundance (%)				$\overline{\chi}^2$ of
$\log_{10}(E/1\,\mathrm{eV})$	p	He	N	Fe	Fit
		QGSJET			
14.5 – 14.9	21.8 ± 0.4	40.1 ± 0.7	23.4 ± 0.7	14.6 ± 0.3	38.1
14.9 – 15.3	42 ± 1	21 ± 2	19 ± 1	18 ± 1	4.5
15.3 – 15.7	51 ± 3	33 ± 4	3 ± 3	13 ± 1	1.9
15.7 – 16.1	53 ± 8	14 ± 10	23 ± 6	10 ± 3	0.7
16.1 – 16.5	31 ± 12	12 ± 18	35 ± 17	22 ± 8	1.9
		VENUS			
14.5 – 14.9	23.9 ± 0.4	27.6 ± 0.7	31.8 ± 0.5	16.7 ± 0.3	47.8
14.9 – 15.3	29 ± 1	29 ± 2	19 ± 1	23 ± 1	5.9
15.3 – 15.7	46 ± 2	23 ± 4	15 ± 3	16 ± 1	1.7
15.7 – 16.1	46 ± 6	6 ± 9	33 ± 7	15 ± 3	0.8
16.1 – 16.5	16 ± 9	33 ± 14	23 ± 13	29 ± 8	1.8
		SIBYLL			
14.5 – 14.9	16.8 ± 0.4	20.9 ± 0.7	24.8 ± 0.7	37.4 ± 0.3	49.4
14.9 – 15.3	35 ± 1	-7 ± 2	39 ± 1	33 ± 1	21.6
15.3 – 15.7	37 ± 3	21 ± 5	9 ± 4	33 ± 2	4.8
15.7 – 16.1	31 ± 6	19 ± 10	9 ± 8	41 ± 4	1.2
16.1 – 16.5	9 ± 9	31 ± 17	8 ± 19	53 ± 11	2.6
		HDPM			
14.5 – 14.9	19.9 ± 0.3	17.9 ± 0.5	31.4 ± 0.5	30.7 ± 0.2	90.0
14.9 – 15.3	19 ± 1	23 ± 1	24 ± 1	34 ± 1	11.5
15.3 – 15.7	32 ± 2	16 ± 3	26 ± 2	26 ± 1	3.2
15.7 – 16.1	37 ± 4	-3 ± 6	43 ± 6	23 ± 3	1.2
16.1 – 16.5	12 ± 6	21 ± 12	18 ± 12	49 ± 8	1.5

Table A.4
Results of the multi-species fits to the CASA-BLANCA data. Statistical errors on each fraction are strongly correlated. The errors increase with energy due to limited statistics. Unphysical negative abundances are a result of a poor hadronic model and/or inadequate statistics.